Extended Passband Bandstop Filter Cascade With Continuous 0.85–6.6-GHz Coverage

Eric J. Naglich, *Student Member, IEEE*, Juseop Lee, *Member, IEEE*, Dimitrios Peroulis, *Member, IEEE*, and William J. Chappell, *Senior Member, IEEE*

Abstract—This paper presents a cascade of tunable bandstop filters with a wide spurious-free upper passband, which is completely spanned by the tuning range of the notch responses. A collection of resonators is shown to be able to provide bandstop filter responses over a 7.8 to 1 tuning range. By using spurious-free upper passband aperture-coupled cavity bandstop filters, multiple resonators, each with octave tuning, can cover a multioctave frequency range in a cascade. It is shown that the upper passband of this type of filter is limited by the reactance of the coupling apertures, which produce an unwanted in-band resonance unless designed properly. The details of this design process are explained and used to design a six-resonator bandstop filter cascade that is able to provide a bandstop filter response with up to 55 dB attenuation over the continuous band of 0.85–6.6 GHz. Through dynamic allocation of the cascade circuit's transmission zeros, one-, two-, three-, and four-pole bandstop filter responses of variable bandwidth can be realized over different frequency ranges, offering numerous bandwidth-attenuation level tradeoff combinations.

Index Terms—Filters, microwave filters, passive filters, tunable filters, tunable resonators.

I. INTRODUCTION

MICROWAVE tunable bandstop filters are important in systems that operate over a wide bandwidth, such as low probability of intercept communications [1], spectrum sensing [2], and dynamic spectral access systems [3]. Due to the wide operating frequency range of these systems, recent bandstop filter research has focused on creating filters that have an extended spurious-free upper passband. In [4], a 6 to 1 upper passband was shown, meaning that the first spurious resonance was at six times the bandstop filter center frequency. An 18 to 1 upper passband was shown in [5], but only in simulation. More recently, two methods to achieve an extended upper passband

were shown in [6]. A tunable bandstop filter with an 8.9 to 1 upper passband was shown in [7].

Previous extended upper passband filters leave systems open to interference over a wide frequency range above the bandstop resonance by design. In some applications, it would be advantageous to implement a bandstop filter with a wide upper passband that could tune over its entire upper passband. Currently, this functionality is usually implemented with yttrium iron garnet (YIG) filter [8] banks. However, YIG filters require a large amount of power ($\geq$1 W) and are physically large compared to some other tunable filter technologies. Solid-state varactor-tuned bandstop filters have been shown to have low power consumption (mW) and very wide tuning ranges (4:1) [9]. However, the use of varactors results in low resonator quality factors (50 or less at microwave frequencies). Microelectromechanical systems (MEMS) tunable bandstop filters [10] offer low power consumption, higher quality factors ($\geq$55 in X-band), and increased power-handling capability compared to some varactor-tuned filters. However, as of now there are no MEMS-tuned bandstop filters with wide upper passbands, and the frequency tuning range of these filters is often less than an octave. One method that has been used to provide a bandstop response over a frequency range wider than the tuning range of a single bandstop filter is a cascade of bandstop filters [11]–[15]. However, a high-quality factor ($\geq$400) low power consumption ($\leq$10 mW) multioctave continuous frequency coverage bandstop filter cascade has not been demonstrated. Therefore, if such filtering capability is desired, there is a need for high-quality (Q) factor resonators that can tune over large frequency ranges with minimal power consumption while maintaining a wide upper passband in a bandstop filter configuration.

Evanescent-mode cavity based filters have been shown to meet most of these requirements [16]. However, past bandstop filters using aperture-coupled cavity resonators [17] do not have wide upper passbands due to the reactance of the coupling apertures. This paper presents a novel method for increasing the spurious-free upper passband of an aperture-coupled cavity bandstop filter. This 7.8 to 1 increased upper passband is combined with the octave tuning range of evanescent-mode cavity resonators to show a high-quality factor ($\geq$400) low power consumption (μW) multioctave continuous frequency coverage bandstop filter cascade for the first time. In addition, the tuning ranges of the component filters of the cascade circuit overlap over designed frequency ranges, allowing higher order notching capability in frequency bands where interference is most expected. This dynamic pole allocation concept is shown graphically in Fig. 1 for a six-resonator bandstop filter cascade.
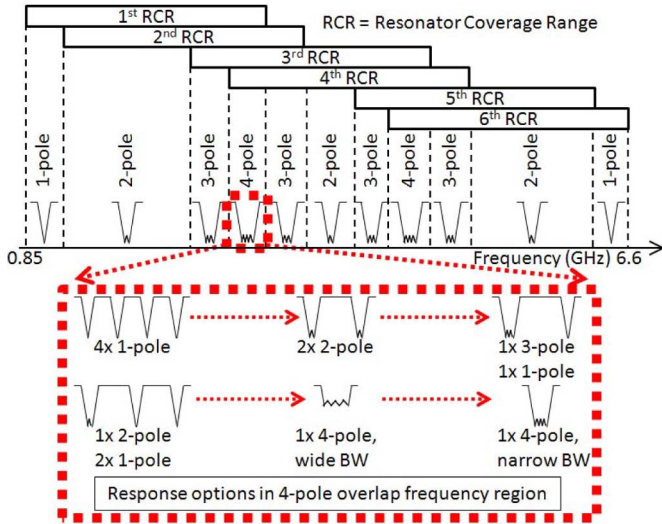
Fig. 1. Concept of a six-resonator bandstop filter cascade using dynamic pole allocation and possible bandstop response orders over a wide spectrum. Examples of six reconfiguration possibilities of a four-pole response are shown in the magnified window with the red (in online version) dotted outline.
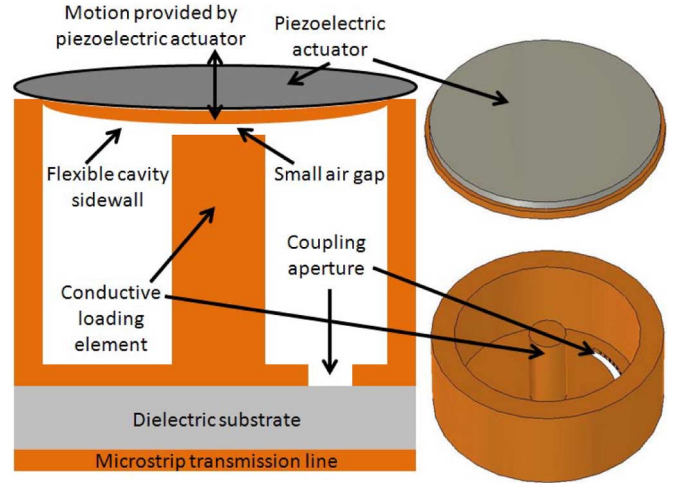

Fig. 2. Illustration of evanescent-mode cavity resonator coupled to a microstrip line through an aperture in the microstrip line's ground plane and a 3-D model of an evanescent-mode cavity resonator.

II. MOTIVATION AND BACKGROUND

Cavity resonators are frequently capacitively loaded in order to reduce their size for a desired resonant frequency [18]. Tunable evanescent-mode cavity resonators are cavity resonators that are very highly capacitively loaded and feature a flexible cavity sidewall above the loading element. The gap between the flexible cavity sidewall and loading element is chosen to be very small relative to the dimensions of the resonator, creating a large capacitance. This capacitance dominates the distributed capacitance of the resonator, and thus the majority of the electric field in the resonator is stored between the loading element and the flexible membrane. Since the majority of the electric field in the resonator is stored in an air dielectric, the resonator has a very high Q (702 at 4.6 GHz, 950 at 17 GHz) [19], [20]. Additionally, since the majority of the electric field is stored in a small volume relative to the resonator size, perturbations to the volume that are small relative to the resonator size can produce very large tuning ranges [16]. For example, in [16], a 3.5 to 1 frequency tuning range is presented with a quality factor of 300–650 across the tuning range. This wide tuning range was accomplished with only 38 μm of flexible cavity sidewall deflection. 38 μm of deflection can be accomplished electronically through the use of commercial piezoelectric actuators [16], electrostatic MEMS actuators [21], or magnetic forces [20]. A conceptual image of a tunable evanescent-mode cavity resonator is shown in Fig. 2 with a piezoelectric actuator for electronic control of the gap between the flexible cavity sidewall and the loading element. In Fig. 2, the resonator is coupled into through an aperture in the ground plane of a microstrip transmission line.

In most bandstop filters, the upper passband limiting factor is spurious higher order resonances of the filter's resonators [7]. Since evanescent-mode cavity resonators are very highly loaded, they have a very wide spurious-free frequency range above their fundamental resonance. This characteristic has been used to create bandpass filters using series-coupled resonators
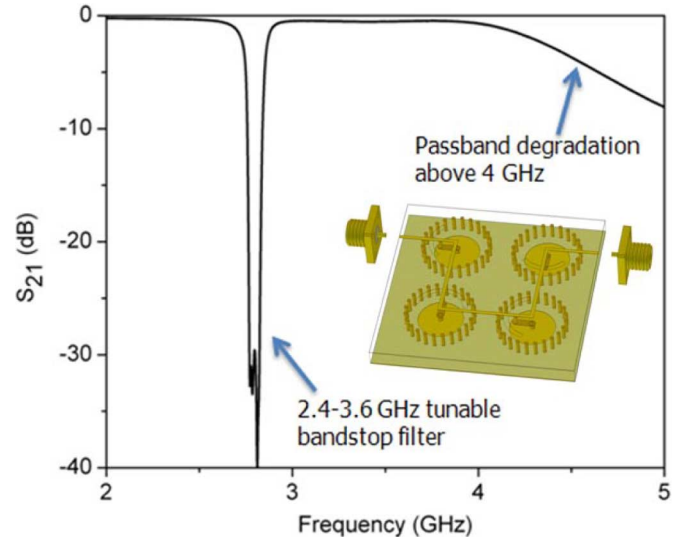

Fig. 3. Measured response of the bandstop filter described in [17] (inset) showing upper passband degradation above 4 GHz.

with very wide spurious-free frequency ranges of 10 to 1 or more [19].

When aperture coupling is used to couple a feeding transmission line to an evanescent-mode cavity resonator in a shunt configuration for a bandstop filter response, as shown in Fig. 2, the coupling apertures are an imperfection in the ground plane of the transmission line. This changes the local characteristic impedance of the transmission line. The local change in characteristic impedance causes reflection of signals at frequencies other than the bandstop filter center frequency, reducing the quality of the bandstop filter's passband. The reflections caused by the coupling apertures are the upper passband limiting factor of aperture-coupled evanescent-mode cavity resonator bandstop filters. An example of this effect can be seen in Fig. 3. Fig. 3 shows a measured response of the four-pole tunable bandstop filter shown in [17] through 5 GHz. While the filter performs well and has a low-loss passband over its tuning range of 2.4 to
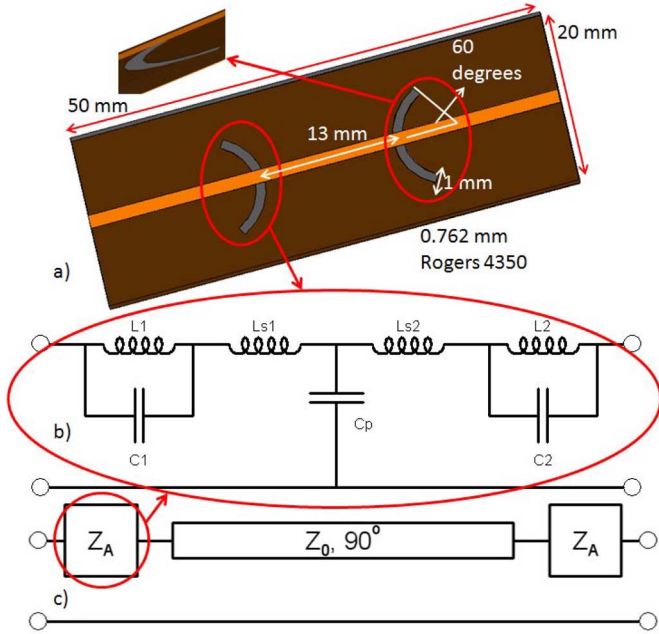
Fig. 4. (a) Illustration of aperture coupling through the ground plane of a microstrip transmission line. (b) Equivalent-circuit model of a coupling aperture. (c) Simplified equivalent circuit of the model in (a).

TABLE I
ELEMENT VALUES FOR EQUIVALENT-CIRCUIT MODEL SHOWN IN FIG. 4(b)

| Inductor	Value (nH)	Capacitor	Value (pF)
L_1	0.501	C_1	0.469
L_2	0.031	C_2	0.301
L_{s1}	0.962	C_p	0.0561
L_{s2}	0.00165		

Fig. 5. (a) Comparison of the lossless circuit-level simulation of an optimized model of the coupling structure in Fig. 4(a), which uses the equivalent-circuit model in Fig. 4(b) and a full-wave simulation of the coupling structure in Fig. 4(a) (metal conductivity = $5.8e7$ S/m, metal thickness = $35\,\mu$m).

3.6 GHz, it can be seen that the passband degrades after 4 GHz. The following sections analyze this effect and provide a new design methodology for extension of the upper passband of aperture-coupled evanescent-mode cavity filters toward the goal of a multioctave coverage bandstop filter cascade.

III. DESIGN OF FEEDING TRANSMISSION LINE AND COUPLING APERTURES

To analyze the effect of the coupling apertures on the upper passband of aperture-coupled evanescent-mode cavity filters, we consider an example of a typical microstrip transmission line with two coupling apertures in its ground plane, as shown in Fig. 4(a). Note that there are no evanescent-mode cavities represented in Fig. 4(a), and the coupling apertures in Fig. 4(a) are not the coupling apertures used in the filter shown in [17]. A microstrip line with apertures in its ground plane can be a bandstop filter itself because the coupling apertures have resonances. It is important to understand that, in this paper, we are using this structure below the first resonance of the coupling apertures. In other words, the below-resonance impedance of the coupling apertures limits the upper passband of the coupling structure in Fig. 4(a) well before the resonances of the coupling apertures limit the upper passband of the structure.

An accurate equivalent-circuit model of an aperture in the ground plane of a transmission line has already been presented [22]. The circuit model described in [22] is repeated in Fig. 4(b) for convenience. The circuit model in Fig. 4(b) models the first two resonances of the coupling aperture and their interaction, which was shown in [22] to accurately model the circuit below resonance. The model is asymmetric because the parallel combination of L_1 and C_1 model the first resonance of the coupling aperture, and the parallel combination of L_2 and C_2 model the second resonance of the coupling aperture. Using this model of
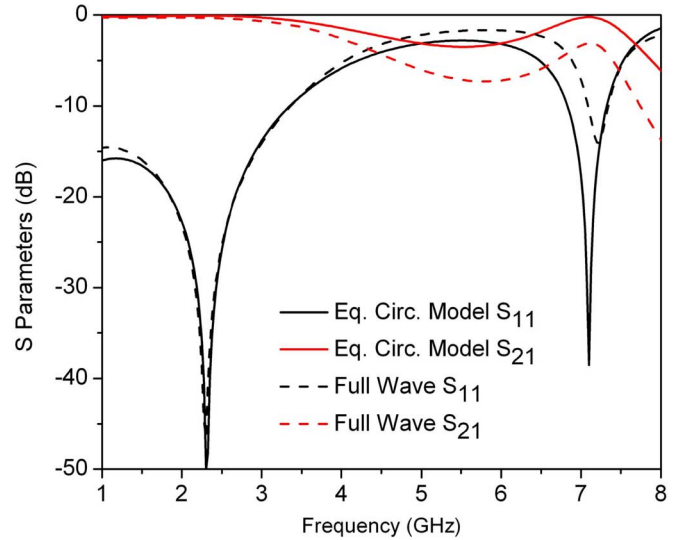
a single aperture, the structure in Fig. 4(a) can be represented as the circuit in Fig. 4(c). Equation [22] describes a method to extract the lumped element values of the circuit model in Fig. 4(b) from full-wave simulation scattering parameter results, and relevant equations from [22] can be found in the Appendix. Full-wave simulation of a single aperture and the entire structure in Fig. 4(a) was done, and lumped-element equivalent-circuit model values were extracted using the method described in [22] and the equations in the Appendix. The equivalent-circuit model extracted values can be seen in Table I. A comparison of the full-wave simulation and the extracted equivalent-circuit lumped-element model response for the models in Fig. 4(a) and (c) is shown in Fig. 5, and good agreement can be seen.

Fig. 5 shows that the microstrip line and coupling apertures shown in Fig. 4(a) have a passband that degrades after 3 GHz, and a spurious bandpass resonance can be seen at 7.1 GHz. Although the spurious bandpass resonance is at 7.1 GHz, its stopband degrades the passband of the coupling structure in Fig. 4(a) at frequencies as low as 3 GHz. This spurious bandpass resonance is at the frequency where the 13-mm transmission line between the coupling apertures in Fig. 4(a) is 180° long. While the transmission line has uniform width across the entire structure, the coupling apertures in its ground plane create inductive impedance boundaries that increase the local characteristic impedance of the transmission line. When a uniform 180° transmission line is terminated in an impedance that does not match its characteristic impedance, a bandpass resonance results. The bandpass resonance at 7.1 GHz in Fig. 5 is due to this effect,
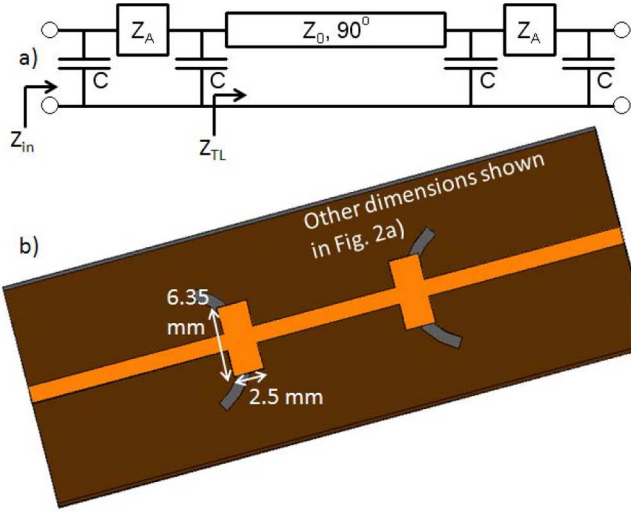
Fig. 6. (a) Equivalent-circuit approximation of aperture coupling through the ground plane of a microstrip transmission line with added shunt capacitance. (b) Illustration of aperture coupling with added capacitive patches on the microstrip line.
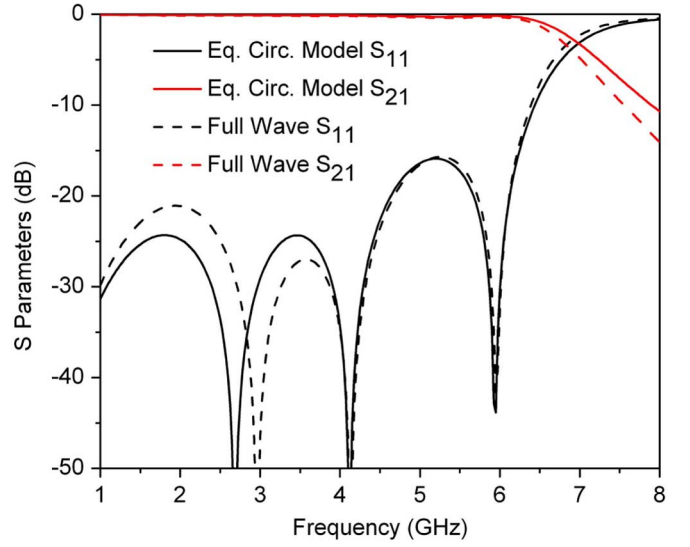

Fig. 7. (a) Comparison of the circuit-level simulation of an optimized model of the coupling structure in Fig. 6(a), which uses the model in Fig. 4(b), and a full-wave simulation of the coupling structure in Fig. 6(b).

and it must be mitigated in order to increase the upper passband of the coupling structure shown in Fig. 4(a).

The proposed method to mitigate the effect of the transmission line bandpass resonance described above is to capacitively load the transmission line section that causes the resonance. Capacitively loading the transmission line resonator reduces its resonant frequency and increases the coupling coefficient into the resonance, making it exhibit a broader response. If the resonance is lowered in frequency and broadened enough, it will become part of the passband of the coupling structure shown in Fig. 4(a). Since the resonance is due to a transmission line, one of the easiest and high quality factor methods to add shunt capacitance to the structure is to use an electrically short length of low characteristic impedance transmission line, similar to what is used in stepped-impedance low-pass filters [23]. The susceptance of a short relatively low characteristic impedance series patch is

$$B = \omega C \approx Y_0 \beta \ell_p \tag{1}$$

where β is the propagation constant, ℓ_p is the length of the patch, C is the shunt capacitance, and Y_0 is the characteristic admittance of the patch.

Models of a transmission line over two coupling apertures with added shunt capacitance in the form of short low characteristic impedance transmission line sections can be seen in Fig. 6, where Z_A is the same as it was in Fig. 4(c). The model in Fig. 6(a) has input impedance of

$$Z_{\mathrm{in}} = \frac{Z_{\mathrm{TL}} + Z_A + j\omega C Z_{\mathrm{TL}} Z_A}{1 + 2j\omega C Z_{\mathrm{TL}} - \omega^2 C^2 Z_{\mathrm{TL}} Z_A + j\omega C Z_A} \tag{2}$$

where

$$Z_{\mathrm{TL}} = Z_0 \frac{\dfrac{1 + j\omega C Z_A}{j\omega C (2 + j\omega C Z_A)} + j Z_0 \tan(\beta\ell)}{Z_0 + j \dfrac{1 + j\omega C Z_A}{j\omega C (2 + j\omega C Z_A)} \tan(\beta\ell)} \tag{3}$$

where C is the shunt capacitance shown in Fig. 6(a), ω is the radian frequency, β is the propagation constant, Z_0 is the characteristic impedance of the transmission line, Z_A is the impedance of the coupling aperture, and ℓ is the length of the transmission line. All of the variables in this equation are known, except for C from either the design of the coupling structure in Fig. 4(a) or parameter extraction from its simulation results. Therefore, (2) can be solved for the value of C that reduces the transmission line bandpass resonance, which occurs when $Z_{\mathrm{in}} = \infty$, to a particular frequency through capacitive loading. The required capacitance can be realized as a low-impedance section of transmission line using (1). Through optimization of (2) to yield an upper passband 1-dB roll-off frequency of 6.5 GHz with minimal passband ripple below 6.5 GHz, the capacitive patches were designed to be 2.5-mm long and 6.35-mm wide, corresponding to a capacitance of 0.85 pF at 4.2 GHz. Fig. 7 shows that the passband of the coupling structure now extends to 6.5 GHz before degradation occurs.

It can be seen that there are two reflection zeros shown in Fig. 5, while there are three reflection zeros shown in Fig. 7. While the reflection zero associated with the bandpass resonance of the transmission line between the coupling apertures (at 7.1 GHz in Fig. 5 and at 6.0 GHz in Fig. 7) is the focus of the proposed extended upper passband technique, the behavior of the other reflection zeros are also well predicted by (2) and are a result of the interaction between the transmission lines of the circuit, the coupling apertures, and the capacitive patches. Since the lower frequency reflection zeros are not the limiting factor of the upper passband of a microstrip transmission line with coupling apertures in its ground plane, (2) provides enough information about their spectral locations in order to optimize the passband. Further understanding of the proposed extended upper passband technique can be gained from examining the passband response for several widths of the capacitive patches in Fig. 6. Fig. 8 shows the S-parameter responses of the coupling structure in Fig. 6 for capacitive patch widths
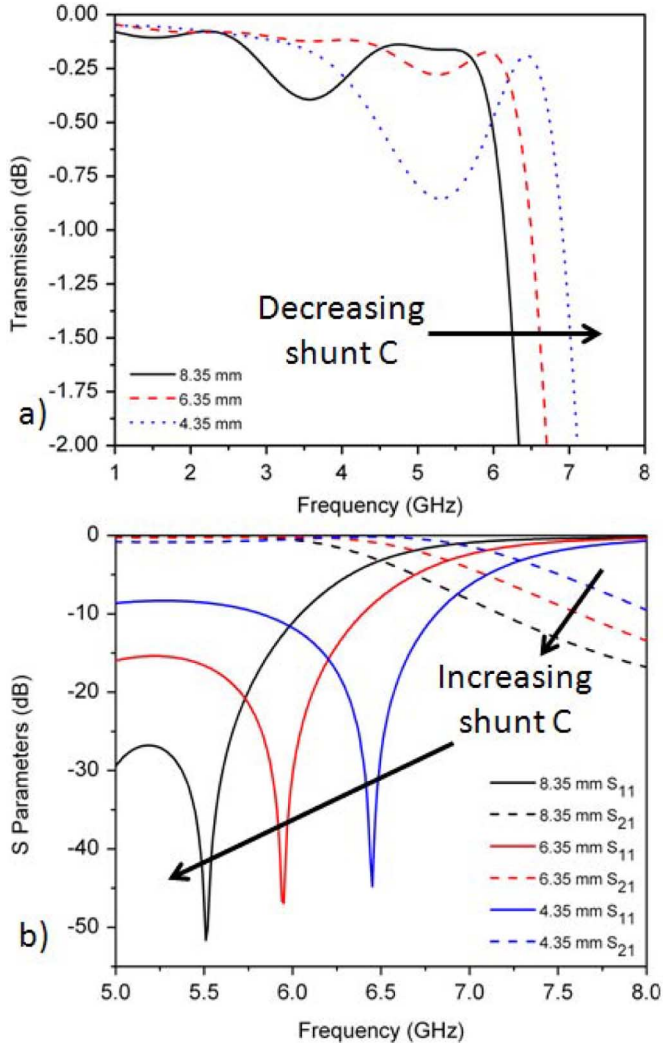
Fig. 8. (a) Transmission response for three widths of the capacitive patch in Fig. 6 showing passband ripple versus passband roll-off tradeoff. (b) S-parameters for three widths of the capacitive patch in Fig. 6 showing the shift of the reflection zero frequency as shunt capacitance is added.

parameters using the method described in [22] and the equations listed in the Appendix.

3) Determine the required value of C for the model in Fig. 6(a) to lower the first transmission line bandpass resonance using (2) so that the passband ripple and roll-off frequency is optimized.

4) Design the capacitive patch dimensions to obtain the capacitance value required from 3) using (1).

5) Optimize the geometry of the capacitive patch in simulation to obtain the desired upper passband shape.

The geometry of the capacitive patch must be optimized in simulation because a low-impedance section of transmission line is not a perfect capacitance. Alternatively, more advanced models of the capacitive patch could be used to further refine its geometry. The wide spurious-free coupling structure response shown in Fig. 7, in addition to the inherent wide spurious-free response of evanescent-mode cavity resonators, provides a path toward very wide frequency coverage bandstop filter cascades.

IV. SIX-RESONATOR BANDSTOP FILTER CASCADE DESIGN

Using the method described in Section III to increase the upper passband of a microstrip line with apertures in its ground plane, an evanescent-mode-cavity-based six-resonator bandstop filter cascade circuit was fabricated in order to provide complete notch coverage of the 0.85–6.6-GHz frequency range. In order to cover the entire frequency range, the six resonators of the structure were segregated into three sets of octave-tunable two-pole filters that each cover a different frequency range. Due to the wide upper passband that is now possible with these filters, they can simply be cascaded. The resonators' tuning ranges were designed to have specific amounts of overlap so that certain portions of the spectrum are able to have two-, three-, and/or four-pole responses. The regions with higher order filter capability can be designed to be in bands where high power or wide bandwidth interference is most expected. An illustration of the fabricated six-resonator bandstop filter cascade can be seen in Fig. 9. The bandstop filter cascade uses three copper layers and two dielectric layers. The top copper layer, labeled Layer 1 in Fig. 9, contains the feeding microstrip transmission line. Capacitive patches can be seen along the length of the line. The top dielectric layer, labeled Layer 2 in Fig. 9, is 0.762-mm-thick Rogers 4350 circuit board material ($\epsilon_r = 3.66$, $\tan(\delta) = 0.0037$ @ 10 GHz). Rectangular regions of this dielectric layer were removed near the input and output ports of the circuit in order to facilitate grounding of the input and output SMA connectors. The middle layer of copper, labeled Layer 3 in Fig. 9, is below the 4350 dielectric layer and serves as the ground plane for the feeding microstrip transmission line. This layer of copper also has semicircular apertures in it for coupling the microstrip transmission line to the evanescent-mode cavity resonators below. The bottom dielectric layer, labeled Layer 4 in Fig. 9, is Rogers TMM3 circuit board material ($\epsilon_r = 3.27$, $\tan(\delta) = 0.002$ @ 10 GHz). The evanescent-mode cavity resonators are integrated into this dielectric layer. The outer walls of the resonators are defined by copper-plated 0.8-mm-diameter via-holes that are spaced close enough together to approximate a solid wall over the circuit's operating frequency range. The resonators use the

of 4.35, 6.35, and 8.35 mm. In Fig. 8(a), the tradeoff between passband ripple and passband roll-off frequency is shown. The 4.35-mm-width case, which adds the least shunt capacitance to the coupling structure, has a higher frequency passband roll-off than the 6.35-mm width chosen in this design, but it also has higher passband ripple. The 8.35-mm-width case, which adds the most shunt capacitance to the coupling structure, has more ripple in the passband than the 6.35-mm-width case, as well as a lower frequency passband roll-off. Fig. 8(b) shows the shift of the reflection zero associated with the bandpass resonance of the transmission line between the coupling apertures as more shunt capacitance is added to the circuit. The location of this reflection zero can be designed to optimize the tradeoff between passband ripple and passband roll-off frequency.

Consequently, the design methodology for the geometry of the proposed capacitive patches can be summarized as follows.

1) Design a conventional aperture-coupled cavity bandstop filter to meet filter shape specifications.

2) Extract the component values for the coupling structure model in Fig. 4(b) from measured or simulated scattering

Fig. 9. Layer-by-layer view of the fabricated six-resonator bandstop cascade.

Fig. 10. Top and bottom views of the fabricated six-resonator bandstop filter cascade.

TABLE II
FABRICATED RESONATOR DIMENSIONS (*: SEE FIG. 9 FOR DEFINITION)

Band	Low	Mid	High
Cavity Radius (mm)	7.5	7	6.75
Loading Post Radius (mm)	1.8	0.62	0.39
Aperture Width (mm)	1	1	1
Aperture Sweep Angle* (degrees)	60	60	50
Cavity Center to Aperture (mm)	5.5	5	5
L* (mm)	7.2	5	2.5
Design Butterworth 10 dB FBW	1%	2.5%	2.5%

bent loading post geometry first shown in [17] to increase coupling for a given coupling aperture size and distance from the feeding microstrip transmission line. A bent loading post geometry redirects the current path in the resonator, which results in a redistribution of the magnetic field in the cavity. By routing the current through the loading post from the center of the cavity toward the outer wall of the cavity, the magnetic field becomes more concentrated on one side of the cavity. If coupling apertures are placed on the side of the cavity with increased magnetic field concentration, stronger coupling into the resonator results. Some of the TMM3 material is removed from the interior of the cavity. These regions can be seen in Fig. 9 as transparent cylinders inside of the cavities and are 2.5-mm deep. The bottom copper layer, labeled Layer 5 in Fig. 9, is a flexible thin sheet over the entire area of the circuit. The copper sheet is attached to the TMM3 dielectric layer everywhere, except within the boundaries of the outer walls of the resonators, creating a bendable membrane over each bent loading post. 0.38-mm-thick half-inch diameter piezoelectric actuators from Piezo Systems Inc. are attached to the side of the bendable copper membranes external to the cavity using silver epoxy. The piezoelectric actuators allow electronic control of the gaps above the bent loading posts in the resonators and the bendable copper membrane. Changing the gaps between the bent loading posts in the resonators changes the capacitance between the top of the loading post and the bendable membrane, which changes the resonant frequency of each resonator.

Images of the fabricated evanescent-mode cavity bandstop filter cascade circuit can be seen in Fig. 10. The wires seen in Fig. 10 are the bias lines for the piezoelectric actuators, which use ±210 V to tune over their entire range of motion. The bias lines are connected to the piezoelectric actuators with silver epoxy external to the cavity. Other than a rectangular patch for
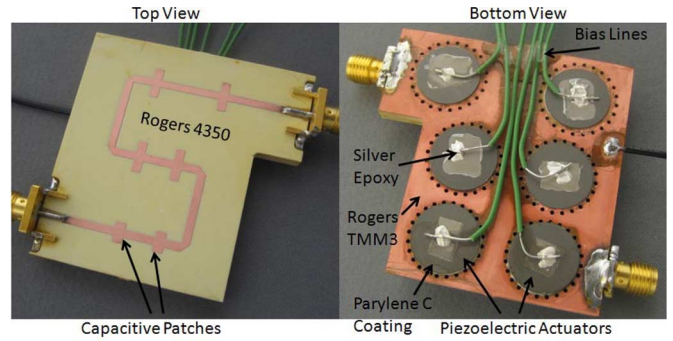
connection of the bias lines, the top and sides of the piezoelectric actuators are coated in Parylene-C from Specialty Coating Systems in order to prevent shorting of the piezoelectric actuator bias voltages to the ground of the filter cascade circuit. In contrast to the four-pole filter in [17] with four similar resonators, the six-resonator cascade circuit shown in Figs. 9 and 10 is divided into three sets of two similar resonators that each focus on a subset of the entire frequency coverage range of the circuit. The dimensions of the resonators can be seen in Table II. While each of the two similar resonators have the same outer diameter and loading post diameter, different nominal gaps between the loading post and the flexible copper membrane allow each resonator to have slightly different tuning ranges.

The length of the transmission lines between the coupling apertures for each of the three two-pole filters are different, as can be seen in Fig. 9. For a frequency-static bandstop filter that uses a transmission line as an inverter between similar resonators, the transmission line should be 90° in electrical length. However, for tunable filters, a transmission line inverter between the resonators can only be 90° in electrical length at one frequency. An asymmetric bandstop response is produced away from this frequency. The transmission line lengths between the resonators were designed in order to have a symmetric response at particular frequencies of interest. Additionally, since the two-pole filters are matched to the system impedance in their passbands, the lengths of transmission line between each two-pole filter do not have an appreciable effect on the cascade's response. Therefore, the transmission lines between each two-pole filter should be kept as short as possible to reduce passband loss. Simulation results of the two lowest frequency resonators in the design, independent of the entire cascade circuit, can be seen in Fig. 11. The resonant frequencies overlap from 1–2 GHz while maintaining an almost 20 dB return loss from 0.5 to 6 GHz. Since the passbands of the individual two-pole
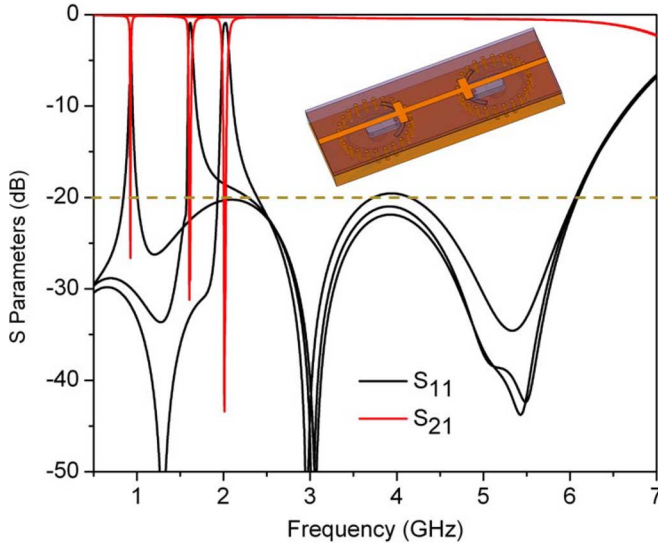
Fig. 11.   Simulated superimposed responses of the two lowest frequency resonators of the cascade design tuning from 1 to 2 GHz while maintaining an almost 20-dB return loss from 0.5 to 6 GHz. The inset shows the simulated structure.

Fig. 13.   Measured versus simulated S_{21} response of the cascade circuit when it is configured to produce three two-pole maximum attenuation responses (static measurement).
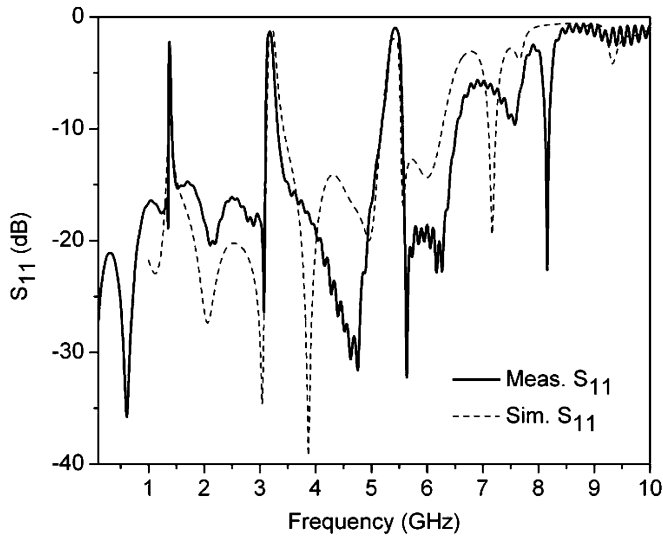

Fig. 12.   Measured versus simulated S_{11} response of the cascade circuit when it is configured to produce three two-pole maximum attenuation responses (static measurement).

Fig. 14.   Bandstop filter cascade circuit measured with all six resonators tuned to independent frequencies, showing the entire one-pole coverage range (static measurement).

filters are able to be well matched over a wide frequency range, component filters of bandstop filter cascades can be designed as individual filters and then simply placed in series. This ease of integration lends itself to modular design, where resonators with a certain coverage range can be dropped into and out of a design for different expected interference scenarios. In addition, it may be possible to increase the upper passband further than what is shown in this paper. This paper manipulates the first bandpass resonance of the transmission line between the coupling apertures in order to increase the upper passband. However, this transmission line has a bandpass resonance at each frequency for which its electrical length is an integer multiple of $180°$. If multiple bandpass resonances of this transmission line could be used to increase the upper passband, the passband could be extended to the first bandstop resonance of the coupling aperture,
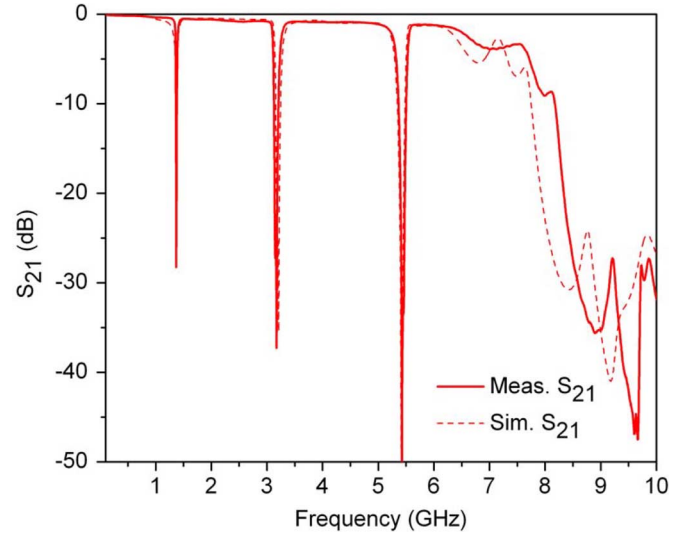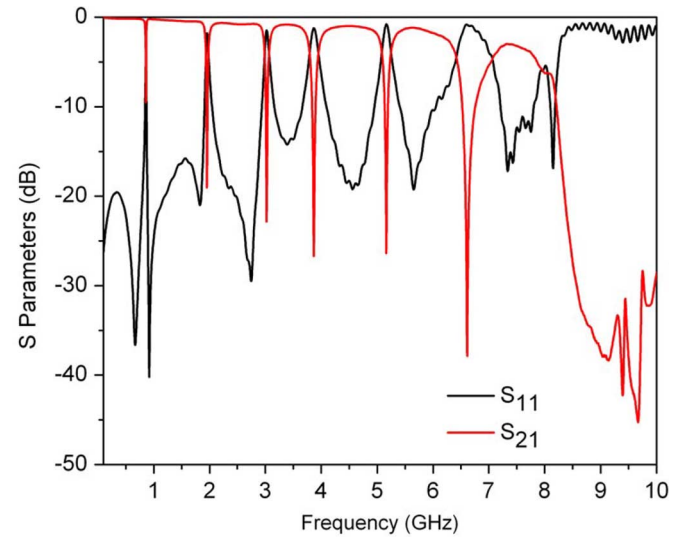
which is much higher than the current limit. For example, the first coupling aperture bandstop resonance for the structure in Fig. 4(a) is at 10.4 GHz. This is a subject of ongoing research.

V. Measured Results

The response of the fabricated bandstop filter cascade was measured using an Agilent Technologies N5230C performance network analyzer (PNA). Bias voltages were applied to the piezoelectric actuators using Keithley 2400 Sourcemeter power supplies. The final structure was simulated using Ansoft High Frequency Structure Simulator (HFSS). Measured versus simulated S_{11} and S_{21} responses can be seen in Figs. 12 and 13, respectively. In both figures, the cascade is configured to produce three two-pole responses. Good agreement can be seen between the measured and simulated data from dc to 6.5 GHz. From 6.5 to 10 GHz, the measured and simulated responses
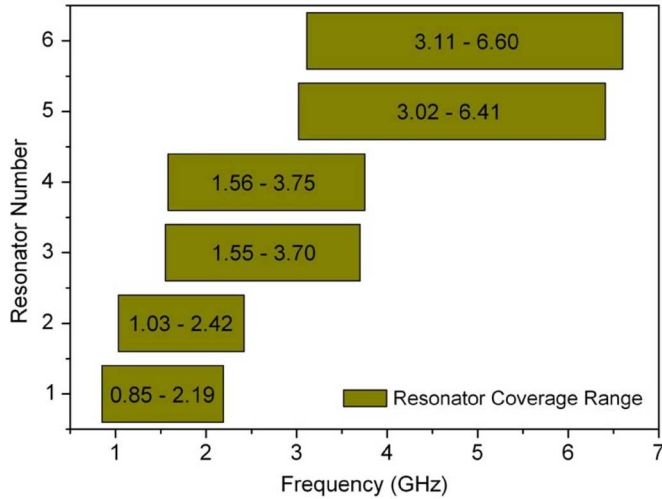
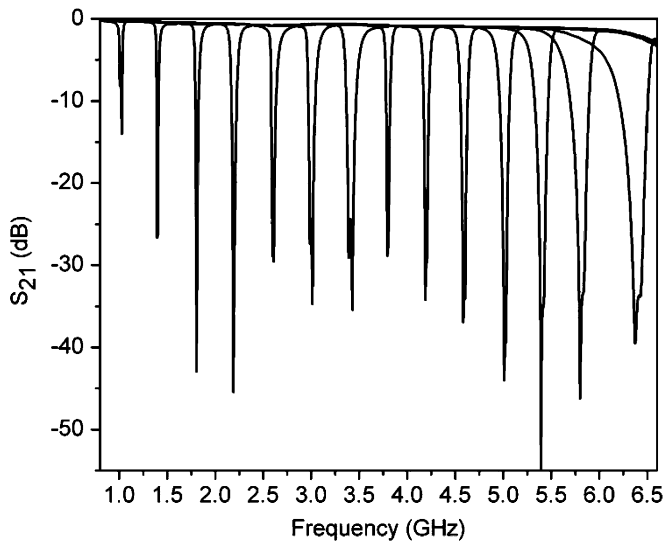Fig. 15. Measured individual resonator tuning ranges.

Fig. 16. Measured superimposed S_{21} responses showing continuous two-pole coverage from 1.03 to 6.4 GHz (tuning measurement).
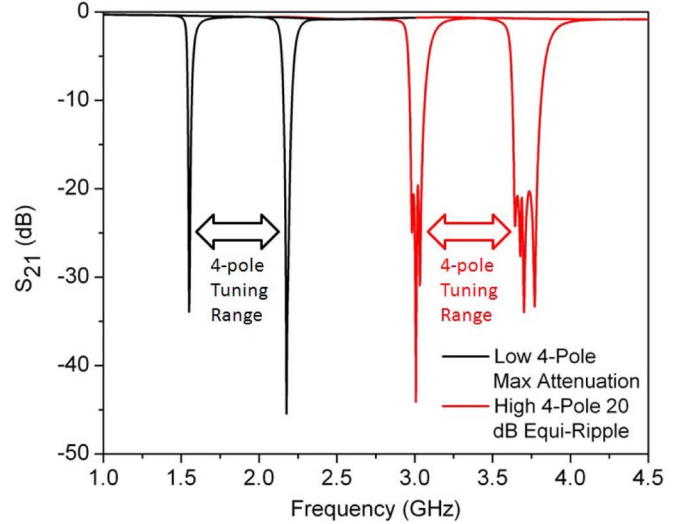

Fig. 17. Measured superimposed S_{21} responses showing the bandstop filter cascade circuit's measured tuning ranges in the four-pole overlap frequency ranges (tuning measurement).
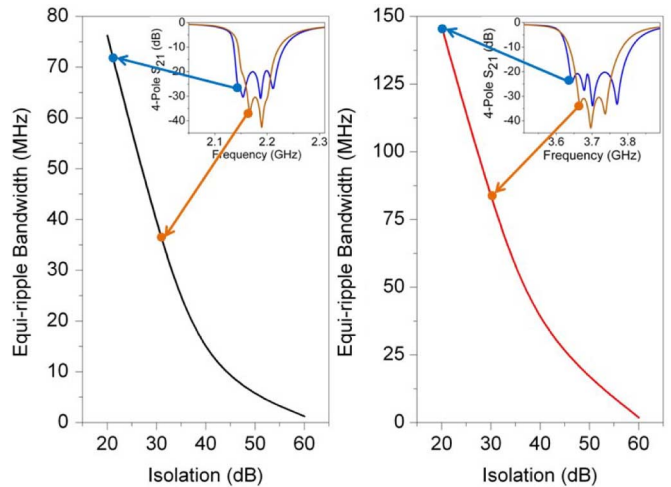

Fig. 18. Measured bandwidth versus equi-ripple attenuation for different shapes of the four-pole filter responses. Insets show examples of 20- and 30-dB levels of attenuation for the four-pole overlap regions of the spectrum.

have similar shapes, but slight discrepancies in frequency. These discrepancies can be explained by slightly smaller coupling apertures than desired and/or slightly smaller capacitive patches than desired according to the equivalent-circuit model described in Section III. The notch responses were measured to have 10-dB fractional bandwidth (FBW) of 1.11% at 1.41 GHz, 2.70% at 3.2 GHz, and 2.57% at 5.41 GHz. The measured passband insertion loss was 0.065 dB at 100 MHz, 0.52 dB at 2 GHz, 0.88 dB at 4 GHz, 1.29 dB at 6 GHz, and 2 dB at 6.5 GHz.

Fig. 14 shows the six resonators tuned to independent frequencies, displaying the complete one-pole coverage range of the bandstop filter cascade. The measured frequency tuning range of each resonator can be seen in Fig. 15. The tuning ranges in Fig. 15 result in frequency overlap ranges covered by multipole responses that can be designed to be in regions of expected interference. For example, the lower frequency range with three- and four-pole coverage is near long-term evolution (∼1.6 and 2.0 GHz), cellular telephone (∼1.8 and 1.9 GHz), and industrial–scientific–medical (ISM) (∼2.4 GHz) signals,

while the upper frequency range with three- and four-pole coverage operates in a common weather and aviation radar band (∼3.1–3.6 GHz). Fig. 16 shows the two-pole coverage range of the cascade circuit, which is 1.03 to 6.4 GHz. Greater than 25 dB of attenuation is shown from 1.5 to 6.4 GHz. The bandwidth changes across the band from 1.0% to 4.8% 10-dB FBW due to the change in electrical length of the coupling apertures across the band. Fig. 17 shows the four-pole coverage ranges of the cascade circuit, which are 1.56–2.19 GHz and 3.11–3.70 GHz. In these regions, multiple filter shapes are possible due to the widely tuning resonators. Fig. 17 shows a Butterworth-like shape in the lower frequency four-pole coverage range and a 20-dB equi-ripple shape in the higher frequency four-pole coverage range. Any filter shape between the two shown, as well as split filter shapes such as two independent two-pole filters, are possible within a four-pole coverage range. This shape reconfigurability allows a dynamic tradeoff between

bandwidth, attenuation level, and number of attenuated bands in the response. Measured results for the tradeoff between bandwidth and equi-ripple attenuation for two frequency tunings of the four-pole filter responses shown in Fig. 17 can be seen in Fig. 18. Examples of more of the possible filter shapes were shown in [17]. Combined with the wide passband and tuning ranges demonstrated in this paper, this high level of filter shape reconfigurability enables unprecedented microwave system robustness in dynamic noisy environments.

VI. CONCLUSION

A method to increase the passband of aperture coupled cavity resonator bandstop filters was described, which used resonances of the transmission lines between coupling apertures. A six-resonator bandstop filter cascade using this method was demonstrated, and a 7.8 to 1 upper passband was obtained. Continuous notch coverage of 0.85–6.6 GHz was achieved within the band. Enabled by the wide tuning ranges of evanescent-mode cavity resonators, the filter shapes and orders across the band could be tuned dynamically. These cascades can be modularly designed, with resonators of different frequency coverage ranges added to or subtracted from the circuit to trade off between attenuation level/response shape flexibility and passband insertion loss due to the length of the feeding transmission line. Bandstop filter cascades like the one demonstrated in this paper are expected to be useful in systems that operate over wide frequency bands in spectral environments with dynamic interference.

APPENDIX
COUPLING APERTURE PARAMETER EXTRACTION FORMULAS

The formulas for parameter extraction of the lumped-element circle values in the model in Fig. 4(b) from measured or simulated S-parameter results, originally derived in [22], are

$$C_i = \frac{1}{Z_0} \cdot \frac{1}{4\pi \Delta f_{3\,\text{dB}\_i}} \tag{4}$$

$$L_i = \frac{1}{(2\pi f_{0i})^2 C_i} \tag{5}$$

$$C_p = -\frac{1}{2\pi f_T X_{21}} \tag{6}$$

$$L_{si} = \frac{X_{ii} - X_{21}}{2\pi f_T} + \frac{L_i}{\left(\frac{f_T}{f_{0i}}\right)^2 - 1} \tag{7}$$

where $i = 1, 2$ represent the first and second resonance of the coupling aperture, f_{01} is the center frequency of the first resonance of the coupling aperture, f_{02} is the center frequency of the second resonance of the coupling aperture, f_T is the frequency of the reflection minimum between the first and second resonance of the coupling aperture, $\Delta f_{3\,\text{dB}_i}$ is the 3-dB bandwidth of the ith resonance of the coupling aperture, and X_{ii} and X_{21} are the imaginary parts of three Z-parameters at f_T.

ACKNOWLEDGMENT

REFERENCES

[1] M. Win and R. Scholtz, "Ultra-wide bandwidth time-hopping spread-spectrum impulse radio for wireless multiple-access communications," *IEEE Trans. Commun.*, vol. 48, no. 4, pp. 679–689, Apr. 2000.

[2] T. Yucek and H. Arslan, "A survey of spectrum sensing algorithms for cognitive radio applications," *IEEE Commun. Surveys Tutorials*, vol. 11, no. 1, pp. 116–130, 2009.

[3] B. Perlman, J. Laskar, and K. Lim, "Fine-tuning commercial and military radio design," *IEEE Microw. Mag.*, vol. 9, no. 4, pp. 95–106, Aug. 2008.

[4] R. Levy, R. Snyder, and S. Shin, "Bandstop filters with extended upper passbands," *IEEE Trans. Microw. Theory Tech.*, vol. 54, no. 6, pp. 2503–2515, Jun. 2006.

[5] N. Yildirim, "Synthesis of bandstop filters with ultra wide upper passbands," in *IEEE MTT-S Int. Microw. Symp. Dig.*, Jun. 2007, pp. 2109–2112.

[6] W. Fathelbab, "Two novel classes of band-reject filters realizing broad upper pass bandwidth;synthesis and design," *IEEE Trans. Microw. Theory Tech.*, vol. 59, no. 2, pp. 250–259, Feb. 2011.

[7] A. Guyette, "Design of fixed- and varactor-tuned bandstop filters with spurious suppression," in *Eur. Microw. Conf.*, Sep. 2010, pp. 288–291.

[8] G. Matthaei, "Magnetically tunable band-stop filters," *IEEE Trans. Microw. Theory Tech.*, vol. MTT-13, no. 2, pp. 203–212, Mar. 1965.

[9] B. Carey-Smith and P. Warr, "Broadband configurable bandstop filter with composite tuning mechanism," *Electron. Lett.*, vol. 40, no. 25, pp. 1587–1589, Dec. 2004.

[10] I. Reines, S.-J. Park, and G. Rebeiz, "Compact low-loss tunable X-band bandstop filter with miniature RF-MEMS switches," *IEEE Trans. Microw. Theory Tech.*, vol. 58, no. 7, pp. 1887–1895, Jul. 2010.

[11] S. Hamzah, B. Ahmad, and P. W. Wong, "Multiband matched bandstop filter," in *IEEE Asia–Pacific. Appl. Electromagn. Conf.*, Nov. 2010, pp. 1–4.

[12] A. Guyette, I. Hunter, and R. Pollard, "Design of absorptive microwave filters using allpass networks in a parallel-cascade configuration," in *IEEE MTT-S Int. Microw. Symp. Dig.*, Jun. 2009, pp. 733–736.

[13] G. Qiu, C. Tsai, B. Wang, and Y. Zhu, "A YIG/GGG/GaAs-based magnetically tunable wideband microwave bandpass filter using cascaded band-stop filters," *IEEE Trans. Magn.*, vol. 44, no. 11, pp. 3123–3126, Nov. 2008.

[14] A. Cismaru and R. Marcelli, "CPW cascaded magnetostatic-wave bandstop resonators," *IEEE Trans. Magn.*, vol. 42, no. 10, pp. 3347–3349, Oct. 2006.

[15] C. Rauscher, "Varactor-tuned active notch filter with low passband noise and signal distortion," *IEEE Trans. Microw. Theory Tech.*, vol. 49, no. 8, pp. 1431–1437, Aug. 2001.

[16] S. Moon, H. Sigmarsson, H. Joshi, and W. Chappell, "Substrate integrated evanescent-mode cavity filter with a 3.5 to 1 tuning ratio," *IEEE Microw. Wireless Compon. Lett.*, vol. 20, no. 8, pp. 450–452, Aug. 2010.

[17] E. Naglich, J. Lee, D. Peroulis, and W. Chappell, "High-Q tunable bandstop filters with adaptable bandwidth and pole allocation," in *IEEE MTT-S Int. Microw. Symp. Dig.*, Jun. 2011, pp. 1–4.

[18] C. Wang, H.-W. Yao, and K. Zaki, "Modeling of conductor-loaded resonators and filters in rectangular enclosures," *IEEE Trans. Microw. Theory Tech.*, vol. 45, no. 12, pp. 2479–2485, Dec. 1997.

[19] H. Joshi, H. Sigmarsson, D. Peroulis, and W. Chappell, "Highly loaded evanescent cavities for widely tunable high-Q filters," in *IEEE MTT-S Int. Microw. Symp. Dig.*, Jun. 2007, pp. 2133–2136.

[20] M. Arif, W. Irshad, X. Liu, W. Chappell, and D. Peroulis, "A high-Q magnetostatically-tunable all-silicon evanescent cavity resonator," in *IEEE MTT-S Int. Microw. Symp. Dig.*, Jun. 2011, pp. 1–4.

[21] X. Liu, L. Katehi, W. Chappell, and D. Peroulis, "High-tunable microwave cavity resonators and filters using SOI-based RF MEMS tuners," *J. Microelectromech. Syst.*, vol. 19, no. 4, pp. 774–784, Aug. 2010.

[22] J.-S. Hong and B. Karyamapudi, "A general circuit model for defected ground structures in planar transmission lines," *IEEE Microw. Wireless Compon. Lett.*, vol. 15, no. 10, pp. 706–708, Oct. 2005.

[23] D. M. Pozar, *Microwave Engineering*, 3rd ed. New York: Wiley, 2005, pp. 412–416.

Eric J. Naglich (S'09) received the B.S.E.C.E. degree from Purdue University, West Lafayette, IN, in 2007, and is currently working the Ph.D. degree in electrical and computer engineering at Purdue University.

From 2007 to 2009, he was with GE Healthcare, where he was involved with electromagnetic subsystem design in medical imaging and surgical navigation machines during the Edison Engineering Development Program. His current research focuses on tunable filter synthesis and fabrication for widely tunable adaptive RF front ends in cognitive radio and radar applications.

Mr. Naglich is a member of the IEEE Microwave Theory and Techniques Society (IEEE MTT-S). He is an officer of Purdue University's Beta Chapter, Eta Kappa Nu. He is a National Defense Science and Engineering Graduate (NDSEG) Fellow. He was the recipient of the Second Place Award of the 2010 IEEE MTT-S International Microwave Symposium Student Paper Competition.

Juseop Lee (A'02–M'03) received the B.E. and M.E. degrees in radio science and engineering from Korea University, Seoul, Korea, in 1997 and 1999, respectively, and the Ph.D. degree in electrical engineering from The University of Michigan at Ann Arbor, in 2009.

In 1999, he joined LG Information and Communications (now LG Electronics), where his activities included design and reliability analysis of RF components for code-division multiple-access (CDMA) cellular systems. In 2001, he joined Electronics and Telecommunications Research Institute (ETRI), where he was involved in designing passive microwave equipment for Ku- and Ka-band communications satellites. In 2005, he joined The University of Michigan at Ann Arbor, where he was a Research Assistant and Graduate Student Instructor with the Radiation Laboratory, during which time his research activities focused on millimeter-wave radars and synthesis techniques for multiple-passband microwave filters. In 2009, he joined Purdue University, West Lafayette, IN, where he is currently a Post Doctoral Research Associate involved with the design of adaptable RF systems. He is listed in *Who's Who in America*. His research interests include RF and microwave components, satellite transponders, and electromagnetic theories.

Dr. Lee was a recipient of the Highest Honor Award presented by Korea University, the Undergraduate Fellowship presented by Korea University, the Graduate Fellowship presented by LG Information and Communications, and the Graduate Fellowship presented by the Korea Science and Engineering Foundation. He was a recipient of the Rackham Predoctoral Fellowship presented by the Rackham Graduate School, The University of Michigan at Ann Arbor. He was also the recipient of the IEEE Microwave Theory and Techniques Society (IEEE MTT-S) Graduate Fellowship. He coauthored the paper that was bestowed the Second Place Award of the 2010 IEEE MTT-S International Microwave Symposium Student Paper Competition.

Dimitrios Peroulis (S'99–M'04) received the Ph.D. degree in electrical engineering from The University of Michigan at Ann Arbor, in 2003.

Since August 2003, he has been with Purdue University, where he currently leads a group of graduate students on a variety of research projects in the areas of RF MEMS, sensing, and power harvesting applications, as well as RF identification (RFID) sensors for the health monitoring of sensitive equipment. He has been a Principle Investigator (PI) or a co-PI in numerous projects funded by government agencies and industry in these areas. He is currently a key contributor in two Defense Advanced Research Projects Agency (DARPA) projects at Purdue that focus on very high-quality ($Q > 1\,000$) RF tunable filters in mobile form factors (DARPA Analog Spectral Processing Program, Phases I, II, and III) and development of comprehensive characterization methods and models for understanding the viscoelasticity/creep phenomena in high-power RF MEMS devices (DARPA M/NEMS S&T Fundamentals Program, Phases I and II). He leads the experimental program on the Center for the Prediction of Reliability, Integrity and Survivability of Microsystems (PRISM) funded by the National Nuclear Security Administration. In addition, he heads the development of MEMS technology in a U.S. Navy project (Marines) funded under the Technology Insertion Program for Savings (TIPS) Program focused on harsh-environment wireless microsensors for the health monitoring of aircraft engines. He has authored or coauthored over 150 refereed journal and conference publications in the areas of microwave integrated circuits, sensors, and antennas.

Dr. Peroulis was the recipient of the 2008 National Science Foundation CAREER Award. His students have been the recipients of numerous Student Paper Awards and other student research-based scholarships. He is a Purdue University Faculty Scholar and has also been the recipient of eight teaching awards including the 2010 HKN C. Holmes MacDonald Outstanding Teaching Award and the 2010 Charles B. Murphy Award, which is the highest undergraduate teaching honor of Purdue University.

William J. Chappell (S'98–M'02–SM'09) received the B.S.E.E., M.S.E.E., and Ph.D. degrees from The University of Michigan at Ann Arbor, in 1998, 2000, and 2002, respectively.

He is currently an Associate Professor with the School of Electrical and Computer Engineering, Purdue University, West Lafayette, IN, where he is also a Member of the Birck Nanotechnology Center and the Center for Wireless Systems and Applications. His research focus is on advanced applications of RF and microwave components. He has been involved with numerous Defense Advanced Research Projects Agency (DARPA) projects involved in advanced packaging and material processing for microwave applications. His research sponsors include the Homeland Security Advanced Research Projects Agency (HSARPA), Office of Naval Research (ONR), the National Science Foundation (NSF), the State of Indiana, Communications–Electronics Research, Development and Engineering Center (CERDEC), and Army Research Office (ARO), as well as industry sponsors. His research group uses electromagnetic analysis, unique processing of materials, and advanced design to create novel microwave components. His specific research interests are the application of very high-quality and tunable components utilizing multilayer packages. In addition, he is involved with high-power RF systems, packages, and applications.

Dr. Chappell was the IEEE Microwave Theory and Techniques Society (IEEE MTT-S) Administrative Committee (AdCom) secretary in 2009. He is a member of the IEEE MTT-S AdCom for 2010–2012.